Holes in the two-dimensional probability density of bistable systems driven by strongly colored noise

G. Debnath* and Frank Moss
Department of Physics, University of Missouri at St. Louis, St. Louis, Missouri 63121

Th. Leiber† and H. Risken
Abteilung für Theoretische Physik, Universität Ulm, D-7900 Ulm, Federal Republic of Germany

F. Marchesoni
Dipartimento di Fisica, Università degli Studi di Perugia, I-06100 Perugia, Italy
(Received 20 February 1990)

Stochastic relaxation in a one-dimensional, bistable potential driven by colored noise ϵ is investigated by means of both numerical codes and analog simulation. By embedding the process under study x into a suitable two-dimensional phase space (x,ϵ), a striking topological effect, observable in the two-dimensional probability density $P(x,\epsilon)$, appears at a critical value of the noise correlation time τ_c. The change of the topology in the neighborhood of τ_c can be characterized as a critical transition. In particular, the top of the potential barrier is shown to give rise to a single saddle in the trajectory space of the embedding process so long as $\tau<\tau_c$. Where $\tau=\tau_c$, however, the single saddle disappears and is replaced by a pair of saddles, which move away from the location of the top of the potential barrier when $\tau>\tau_c$, leaving behind a concave depression or "hole" in the probability density. The relevance of this observation to the problem of calculating the mean first-passage time for particle escape from one well to the other at large τ is discussed in detail. A complete analytical description of this transition has defied all attempts thus far. Consequently, many interesting open questions remain.

I. INTRODUCTION

The stochastic relaxation of particles in bistable systems driven by colored noise plays a major role in a number of problems in statistical mechanics and in synergetics. A great deal of work has been devoted to this problem; see, for instance, Refs. 1–4 for reviews. The simplest case is described by the stochastic differential equation

$$\dot{x}=-f'(x)+\epsilon(t)\ , \tag{1.1}$$

where $f(x)$ is a bistable potential and $\epsilon(t)$ an external Gaussian stochastic force with zero mean and correlation function,

$$\langle\epsilon(t)\rangle=0;\quad\langle\epsilon(t)\epsilon(s)\rangle=\frac{D}{\tau}\exp\left[-\frac{|t-s|}{\tau}\right]\ . \tag{1.2}$$

In the limit of vanishing noise correlation time $\tau\to 0$, the correlation function in (1.2) reduces to the white-noise δ-function

$$\langle\epsilon(t)\epsilon(s)\rangle=2D\delta(t-s)\ .$$

The problem of mean-first-passage times and other problems in bistable potentials have been studied for many years, starting with the pioneering work of Kramers.[5] Investigations beyond the white-noise limit have first focused on the small-τ regime.[6] In first order in τ, the distribution function $P(x)$ still obeys a bona fide one-dimensional Fokker-Planck equation. The investigation for the white noise case can thus be carried over to the short correlation time regime.[7–9]

For larger correlation times it seems to be more appropriate to consider a two-dimensional process. The noise $\epsilon(t)$ is now considered to be a variable obeying the stochastic differential equation

$$\dot{\epsilon}(t)=-\frac{1}{\tau}\epsilon(t)+\frac{1}{\tau}\Gamma(t)\ , \tag{1.3}$$

where $\Gamma(t)$ is the usual white-noise force

$$\langle\Gamma(t)\rangle=0,\quad\langle\Gamma(t)\Gamma(s)\rangle=2D\delta(t-s)\ . \tag{1.4}$$

Equations (1.3) and (1.4) describe an Ornstein-Ulhenbeck process with correlation function (1.2). Thus the process under consideration can as well be described by the two Langevin equations (1.1) and (1.3) with the white-noise force (1.4). Instead of the one-dimensional probability density we may now look for the two-dimensional density $P(x,\epsilon,t)$. It follows from the Langevin equations (1.1) and (1.3) that $P(x,\epsilon,t)$ obeys the two-dimensional Fokker-Planck equation (FPE)

$$\frac{\partial P(x,\epsilon;t)}{\partial t}=L(x,\epsilon)P(x,\epsilon;t)\ , \tag{1.5a}$$

$$L(x,\epsilon)=\frac{\partial}{\partial x}f'(x)-\epsilon\frac{\partial}{\partial x}+\frac{1}{\tau}\frac{\partial}{\partial\epsilon}\left[\epsilon+\frac{D}{\tau}\frac{\partial}{\partial\epsilon}\right]\ . \tag{1.5b}$$

Many publications deal with the problem of the mean-

first-passage time (MFPT) in bistable systems driven by colored noise.[6] In particular, the dependence of the MFPT on the correlation time for intermediate τ and asymptotic expressions for large τ have been derived recently.[10–15] The main message of these investigations seems to be that the MFPT decreases exponentially with increasing correlation time.

Only very few investigations are concerned with the stationary probability density $P(x,\epsilon)$. By numerically solving the FPE, (1.5), with the matrix-continued-fraction (MCF) method[16] and the Langevin equations (1.1) and (1.3) with analog simulation techniques,[17] $P(x,\epsilon)$ has been determined for the quartic potential,

$$f(x)=-\frac{a}{2}x^2+\frac{b}{4}x^4 , \tag{1.6}$$

for values of $\tau \leq 1$. The distributions thus obtained show a single saddle point at $x=0$ and $\epsilon=0$ and two maxima located symmetrically in the plane (x,ϵ) in correspondence with the potential minima. As was first discovered by analog simulation techniques,[18] the topology of $P(x,\epsilon)$ changes drastically when τ exceeds a certain critical value τ_c, which depends on the noise intensity D. A precise determination of the critical behavior of the process described by Eqs. (1.1) and (1.3) in the close neighborhood of τ_c, however, requires the implementation of accurate numerical tools such as the MCF algorithm.[3]

We have previously presented evidence that the colored-noise-induced topological transition discussed here occurs for a variety of bistable and multistable potential shapes, including even a random potential.[19] We decided to carry out our numerical analysis for the bistable, periodic potential,

$$f(x)=-a\cos(x)+b\cos(2x) , \tag{1.7}$$

which had been introduced previously[10] to calculate the dependence of the MFPT on the noise correlation time.

The reason for the choice of the system given by Eq. (1.7) rather than Eq. (1.6) is merely numerical: The MCF algorithm employed throughout the present work converges much faster when a Fourier expansion of $P(x,\epsilon,t)$ is possible.[3] The convergence achieved for the periodic, bistable potential allowed us to obtain accurate contours of constant stationary probability at sufficiently large values of $\tau > \tau_c$. As a consequence, we were able to obtain the positions of the off-axis saddle points with high precision and to investigate in detail the dependence of τ_c on the noise intensity D.

The present paper is organized as follows: In Sec. II we demonstrate the occurrence of the topological transitions in the presence of colored noise for both the periodic and the quartic double-well potential by means of the MCF algorithm and analog simulation, respectively. In Sec. III, we characterize the critical nature of the process in the neighborhood of τ_c, and we describe the asymptotic behavior for $\tau \gg \tau_c$. The connection of the phenomenon investigated here with the problem of the MFPT for large τ is discussed in Sec. IV.

II. TOPOLOGICAL EFFECTS INDUCED BY COLOR

The existence of topological effects induced by strongly correlated noise has been pointed out first in Ref. 18 for a "soft" potential, so called because of its linear behavior in the limit of large displacement. Since that time, evidence has been obtained that such effects are generic to any bistable or multistable potential, irrespective of its asymptotic behavior. Even spatially random potentials exhibit such properties.[19] In this section, we study two potentials in detail: the periodic bistable potential, Eq. (1.7), for which the FPE has been solved by means of the MCF algorithm of Ref. 3; and the quartic double-well potential, Eq. (1.6), the dynamics of which has been simulated by an analog electronic circuit.[20] In the following, we demonstrate the occurrence of color-induced topological effects for both families of potentials. We also exhibit the critical nature of this phenomenon. This transition, to be sure, occurs in the two-dimensional stationary probability density but is otherwise very similar to the one-dimensional noise-induced transitions discussed by Horsthemke and Lefever.[21]

A. The periodic bistable potential

The potential defined by Eq. (1.7) is plotted in Fig. 1 for $a=0.5$ and $b=1.0$. Our discussion in a sequel will make use of the following parameters which characterize the potential: (a) the stable and unstable fixed points,

$$x_0=\pm\cos^{-1}\left[\frac{a}{4b}\right], \quad x_u=0,\pm\pi ; \tag{2.1}$$

(b) the curvature of the potential $f(x)$ in the neighborhoods of x_0 and $x_u=0$,

$$\omega_0=f''(x_0)=4b-\frac{a^2}{4b}, \quad \omega_u=|f''(0)|=4b-a ; \tag{2.2}$$

and (c), the height of the barrier at $x_u=0$ and $x_u=\pm\pi$,

$$\Delta f(0)=f(0)-f(x_0)=2b-a+\frac{a^2}{8b} , \tag{2.3a}$$

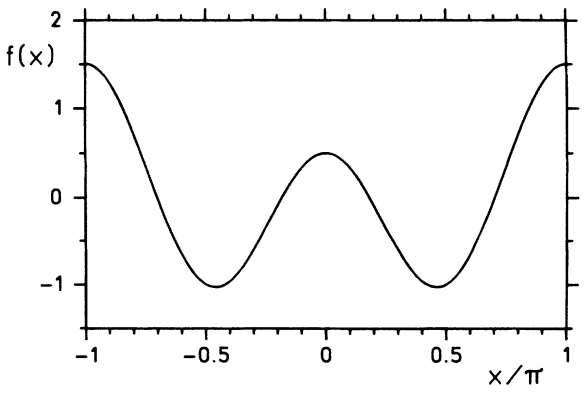

FIG. 1. The periodic bistable potential of Eq. (1.7) for $a=0.5$ and $b=1.0$.

$$\Delta f(\pm\pi)=f(\pm\pi)-f(x_0)=2b+a+\frac{a^2}{8b} . \quad (2.3b)$$

All calculations reported here were made for the following parameter values: $a=0.5$, $b=1.0$, $x_0\cong\pm 0.46\pi$, $\omega_0=\frac{63}{16}$, $\omega_u=\frac{7}{2}$, $\Delta f(0)=\frac{49}{32}$, and $\Delta f(\pm\pi)=\frac{81}{32}$.

The boundary conditions for the corresponding FPE, (1.5), were set as follows:

$$P(x+2\pi,\epsilon;t)=P(x,\epsilon;t) , \quad (2.4a)$$

$$\lim_{\epsilon\to\pm\infty} P(x,\epsilon;t)=0^+ . \quad (2.4b)$$

The reason for choosing the periodic boundary condition, Eq. (2.4a) has been explained in Ref. 10. Any time the random walker associated with the coordinate $x(t)$ jumps over the potential barrier at $x_u=\pm\pi$, it is reinjected at the opposite potential barrier at $x_u=\mp\pi$, so that the only detectable hopping mechanism between the potential barrier at $x_u=\mp\pi$, so that the only detectable hopping mechanism between the potential wells at x_0 takes place across the lower barrier at $x_u=0$. In this respect, the periodic potential, Eq. (1.7), is a good surrogate for a bistable potential, provided that $D\ll\Delta f(0)$.[10]

Solving the FPE, (1.5), for the periodic bistable potential, Eq. (1.7), with the boundary conditions given by Eq. (2.4), is equivalent to determining the *discrete* eigenvalues and eigenfunctions of the relevant spectral problem,

$$L(x,\epsilon)P(x,\epsilon)=-\lambda P(x,\epsilon) . \quad (2.5)$$

The stationary probability distribution,

$$P_{\rm st}(x,\epsilon)\equiv\lim_{t\to\infty} P(x,\epsilon;t) ,$$

coincides with the eigenfunction $P_0(x,\epsilon)$ corresponding to $\lambda=0$. The contour lines of $P_0(x,\epsilon)$ for one value of the noise intensity are displayed in Fig. 2. On increasing τ from zero, the double-peaked structure of $P_0(x,\epsilon)$ is first twisted clockwise, and then the single saddle at the origin is suddenly replaced by a local minimum or "hole." Simultaneously, the single saddle branches into a pair of symmetric, off-axis saddles which move farther apart upon further increases in τ. We denote the coordinates of these new saddle points by

$$s_\pm=(x_s(\tau),\epsilon_s(\tau)) .$$

For extremely large values of τ $s_\pm(\tau)$ appears to approach two asymptotic fixed points $s_\pm(\infty)$, while the corresponding value of $P_0(x_s,\epsilon_s)$ becomes vanishingly small. However, the depth of the hole, measured by the ratio $P_0(x_s,\epsilon_s)/P_0(0,0)$, increases with τ. Note that typically $P_0(x_s,\epsilon_s)$ is orders of magnitude smaller than the off-axis[10] peaks of $P_0(x,\epsilon)$.

The topological effect we have observed is a critical transition in that, at a given noise intensity, it only appears for τ greater than some threshold value τ_c and *vice versa*. In Fig. 3 we plot the phase plane, wherein the critical values D_c and τ_c lie on a line dividing the two topological behaviors. The critical value τ_c appears in both the numerics and the analog simulations to exhibit a definite positive lower bound τ_0. It is worth emphasizing,

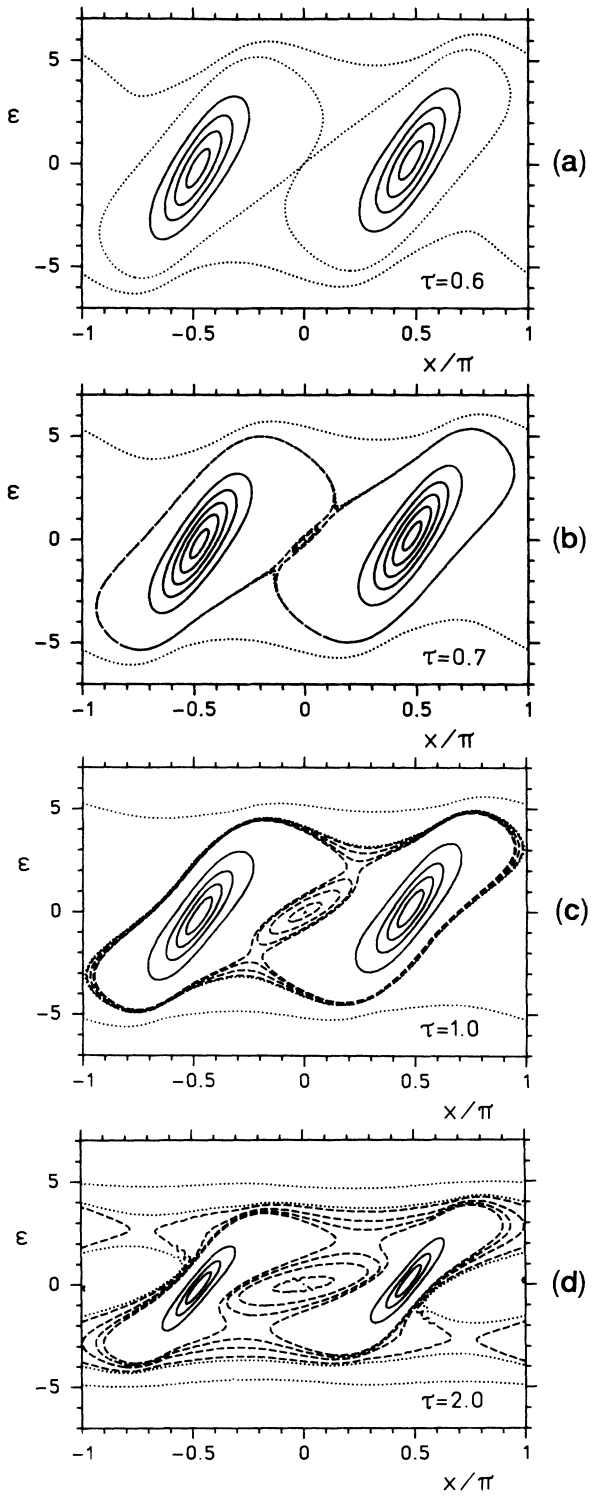

FIG. 2. $P_0(x,\epsilon)$ contour lines for the potential shown in Fig. 1 at fixed noise intensity $D=3$. The probability values of the contour lines were chosen to emphasize the hole at the origin. They are as follows. (a) Dotted: 1.31 and 3.77×10^{-3}; solid: 3, 6, . . . , 12×10^{-2}. (b) Dotted: 1.01 and 3.21×10^{-3}; solid: 3, 6, . . . , 15×10^{-2}. (c) Dotted: 4.4 and 19.4×10^{-4}; dashed: 2, 2.2, 2.4, and 2.5×10^{-3}; solid: 3, 9, . . . , 21×10^{-2}. (d) Dotted: 2.2 and 28.1×10^{-5}; dashed: 4,8, . . . , 16×10^{-4}; solid: 0.1, 0.3, and 0.5.

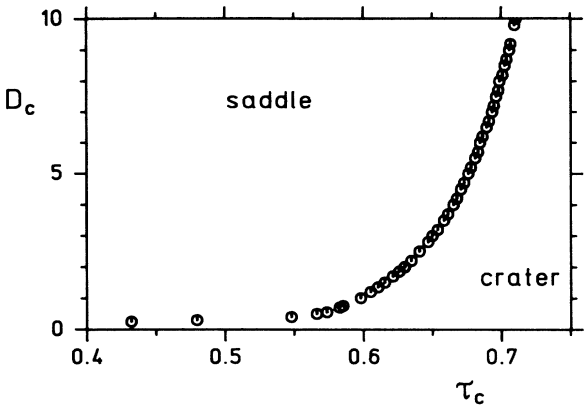

FIG. 3. The phase plane, D_c vs τ_c, for the potential shown in Fig. 1.

however, that *the existence of τ_0 is one of the few predictions which we have been able to prove analytically.* An additional feature shown by Fig. 3 is the kink represented by the abrupt change in slope of the curve $D_c(\tau_c)$ near $\tau_k \cong 2\tau_0$. We shall further discuss the critical nature of the mechanism responsible for the bifurcation of the single saddle into the off-axis pair $s_\pm$ in Sec. III.

B. The quartic double-well potential

The potential given by Eq. (1.6) is plotted in Fig. 4 for $a=b=1.0$. This potential exhibits two stable points and one unstable fixed point at x_0, where $x_0=\pm\sqrt{a/b}$, and $x_u=0$, respectively. The curvatures at x_0 and x_u are given by $\omega_0=f''(x_0)=2a$, and $\omega_u=|f''(0)|=a$. The barrier height is

$$\Delta f(0)=f(0)-f(x_0)=a^2/4b \ .$$

The dynamics of the process defined by Eqs. (1.1) and (1.2) was simulated with an analog electronic circuit using by now well-developed techniques.[20] After simultaneously sampling the trajectories $x(t)$ and $\epsilon(t)$ for sufficiently long times, the stationary distribution $P_0(x,\epsilon)$ was determined to reasonably good accuracy. Typically, the trajectories were digitized into 1000-point samples each, and 1000–2000 such samples were obtained. The final distribution thus was built up from 2 to 4 million digitized points. The resulting statistical errors in P_0 were small enough that the main features of the topological transition could easily be observed, though in the close neighborhood of the $D_c(\tau_c)$ curve only the MCF method was sufficiently accurate to explore the critical features in detail. In Fig. 5 we display some measured cross sections

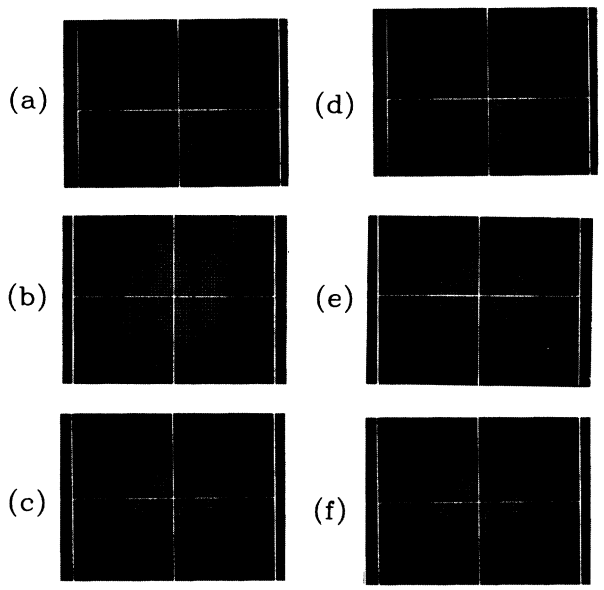

FIG. 5. $P_0(x,\epsilon)$ cross section through the saddle point for the potential shown in Fig. 4 measured on the analog simulator for $\tau=5$: (a) $D=2.2>D_c$, (b) $D=2.1\cong D_c$, and (c) $D=0.45<D_c$; and for $\tau=10$: (d) $D=48.4>D_c$, (e) $D=22.5\simeq D_c$ and (f) $D=6.4<D_c$.

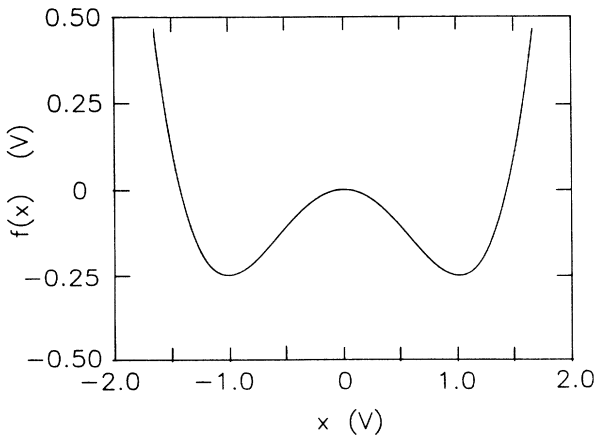

FIG. 4. The quartic double-well potential of Eq. (1.6) for $a=b=1.0$.

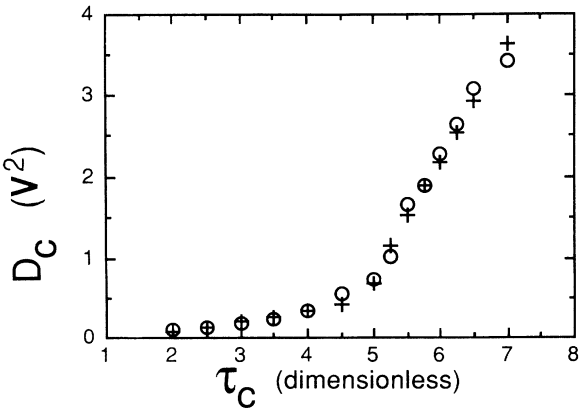

FIG. 6. The phase plane measured by analog simulation for the potential of Eq. (1.6) with $b=1$ and $a=0.82$ (circles) and $a=0.72$ (crosses).

through $P_0(x,\epsilon)$ for two fixed values of the noise correlation time and increasing values of intensity. The cross sections have been chosen close to the saddle point(s). The appearance of the hole in the probability distribution is clearly evidence when the noise intensity is larger than some threshold value which itself increases with τ. We verified that the dependence of this effect on τ and D exhibits the very same features which we demonstrated for the periodic bistable potential. In particular, our data for D_c and τ_c as shown in Fig. 6 are consistent with the previous MCF observations though not as accurate. No holes were observed for τ smaller than a certain threshold τ_0, no matter how weak the noise intensity. The kink in the $D_c(\tau_c)$ curve, seen earlier using the MCF algorithm with the periodic bistable potential, is here also clearly evident.

III. CRITICAL BEHAVIORS

We discuss here the implications of the most remarkable features of the mechanism under study. This discus-

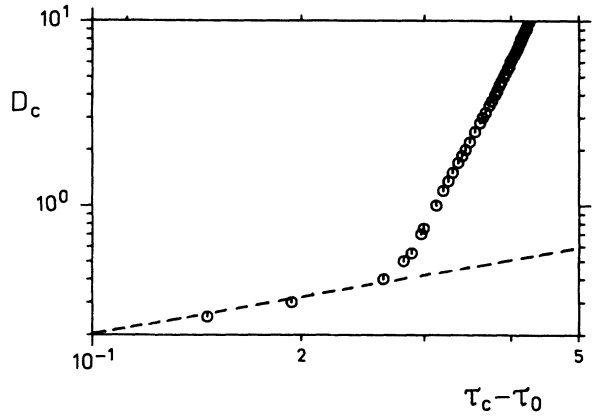

FIG. 7. D_c vs $\tau_c-\tau_0$ on a log-log plot. The data are taken from Fig. 3. A line of slope 1 (dashed) is shown for comparison.

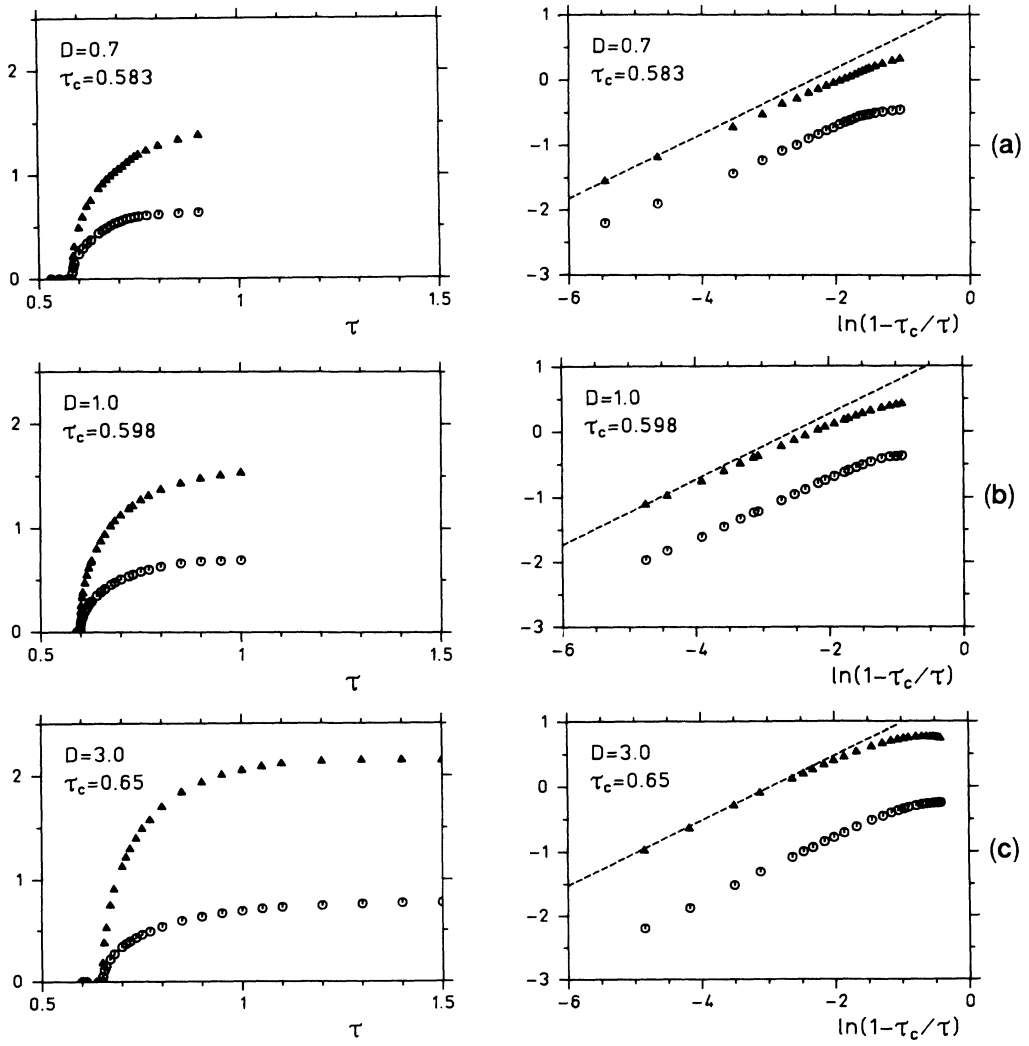

FIG. 8. $x_s(\tau)$ (circles) and $\epsilon_s(\tau)$ (triangles) on linear scales (left) and logarithmic scales (right) for three values of D (a)–(c) for the potential shown in Fig. 1. The dashed curves represent the law given by Eq. (3.5) for ϵ_s with the critical exponent set equal to $\frac{1}{2}$.

sion is based largely on the MCF results for the periodic bistable potential for two reasons: First, and most significant, it seems very difficult to obtain comprehensive analytical results, and consequently we have not yet been able to develop such a theory. Second, only the MCF results are sufficiently accurate to closely examine the critical behavior.

A striking result, introduced in Sec. II, is that the single saddle in the probability density $P_0(x,\epsilon)$ at the origin bifurcates to a symmetrically located, off-axis pair as the critical line, $D_c(\tau_c)$, is crossed for increasing τ or decreasing D, and that there is some threshold $\tau_0>0$ at which the critical line terminates. Though the former part of this statement seems to defy analytical procedures, the latter can be rigorously justified. Let us recall that any extremal point of $P_0(x,\epsilon)$ designated by $e=(x_e,\epsilon_e)$, is determined by the requirements

$$\frac{\partial}{\partial x}P_0(x,\epsilon)\bigg|_e=\frac{\partial}{\partial\epsilon}P_0(x,\epsilon)|_e=0\ . \tag{3.1}$$

Substituting Eq. (3.1) into the FPE, (1.5), yields

$$\frac{\partial^2}{\partial\epsilon^2}P_0\bigg|_e=-\frac{\tau^2}{D}\left[f''(x_e)+\frac{1}{\tau}\right]P_0\bigg|_e\ . \tag{3.2}$$

Let us suppose that $P_0(x,\epsilon)$ can be expanded in a Taylor double-power series in the neighborhood of (x_e,ϵ_e). The analyticity of $P_0(x,\epsilon)$ was understood when we adopted the MCF algorithm of Ref. 3 to solve Eq. (1.5). That such solutions are comparable with the results of analog simulations supports our assumption. The left-hand side of Eq. (3.2) is the curvature of $P_0(x,\epsilon)$ parallel to the ϵ axis at the extremal point and, of course, $P_0(x_e,\epsilon_e)$ is positive definite. Let us now identify the extremal point e with the origin. For (0,0) to become a local minimum of $P_0(x,\epsilon)$, $(\partial^2/\partial\epsilon^2)P_0|_{(0,0)}$ must become positive or, equivalently, the factor in large parentheses in Eq. (3.2) must change sign. This condition allows us to determine analytically the minimum τ value, τ_0, for the appearance of the hole in the distribution:

$$\tau_0=-[f''(0)]^{-1}=\omega_u^{-1}\ . \tag{3.3}$$

This prediction compares very well with both numerical (Fig. 3) and analog simulation (Fig. 6) results. Within the accuracy of the two methods, it becomes evident that τ_c approaches τ_{0^+} for vanishingly small values of D_c. A similar observation of a threshold in the noise correlation time has been made in the context of the breakdown of the small τ expansion by Tsironis and Grigolini.[11]

Determining the analytic dependence of D_c on τ_c turns out to be an extremely challenging problem, wherein the nonlinear nature of the process plays a dominant role. Because of this it may be advantageous to manipulate the data in various ways. For example, recalling that $\tau_c\geq\tau_0$, we have replotted the data from Figs. 3 and 6 on suitable logarithmic scales as shown in Fig. 7. For both potentials, D_c seems to be proportional to $\tau_c-\tau_0$ for $\tau_c<\tau_k$, whereas it increases much more rapidly for $\tau_c>\tau_k$. The location of the kink in the $D_c(\tau_c)$ curve, τ_k, varies with the actual shape of the potential $f(x)$ (see Figs. 3 and 6).

In Sec. II we also showed how, at $\tau=\tau_c$, the single saddle point bifurcates to two off-axis saddle points $s_\pm$, which, on further increasing τ, move to two symmetric fixed points $s_\pm(\infty)$. Moreover, the probability distribution at $s_\pm$ vanishes asymptotically for $\tau\to\infty$, but at a slower rate than at the origin. The dependence of x_s on τ can be explained from this piece of information as a natural consequence of the discussion following Eq. (3.2). Let us rewrite[15] $P_0(x,\epsilon)$ as $\exp[-\phi(x,\epsilon)]$. At the saddle points $(\partial/\partial\epsilon)\phi|_{s_\pm}=0$, and, see Eq. (3.2)

$$\frac{\partial^2}{\partial\epsilon^2}\phi\bigg|_{s_\pm}=\frac{\tau^2}{D}\left[f''(x_s)+\frac{1}{\tau}\right]\ .$$

As $\tau\to\infty$, $P_0(x,\epsilon)$ shrinks into two δ functions centered at $\pm(x_0,0)$, while at the off-axis saddle points $s_\pm(\infty)$, seem to flatten out and eventually vanish. (See Fig. 2.) This requirement leads to the simple prediction $x_s(\infty)\equiv\tilde{x}_\infty$, where $\tilde{x}_\infty$ is the positive solution of the equation, $f''(\tilde{x}_\infty)=0$.

In Fig. 8, we report our numerical determination of $x_s(\tau)$ and $\epsilon_s(\tau)$ for the periodic bistable potential shown in Fig. 1. The bifurcation of the saddle point (0,0) into the symmetric saddle points $s_\pm$ is clearly characterized by a pitchfork-type curve for both coordinates. The off-axis branches of such curves appear to take on asymptotic values $\pm x_s(\infty)$ and $\pm\epsilon_s(\infty)$, respectively. For $\tau\gg\tau_c$, $x_s(\tau)$ approaches $\tilde{x}_s(\infty)$ fairly closely. There is, however, an overshoot effect which is present for large enough D, whereupon $x_s(\tau)$ first exceeds the asymptote, then approaches it from above. For small D, the approach is always from below the asymptote.

A similar check has been carried out for the quartic double-well potential, leading to the same conclusions even though with less compelling accuracy. Consistently, all the computations and simulations which we have performed seem to suggest that $(\partial^2/\partial\epsilon^2)P_0|_{s_\pm}$ becomes negative for τ large enough. (See Figs. 2 and 9.) In fact, this implies that $\tau f''(x_s)>-1$ for $\tau\gg\tau_c$, or equivalently, $x_s(\tau)>\tilde{x}(\tau)$, where $\tilde{x}(\tau)$ is given by

$$\tau f''(\tilde{x}(\tau))+1=0\ , \tag{3.4}$$

with $\tilde{x}(\tau_0)=0$ and $\tilde{x}(\infty)=\tilde{x}_\infty$.

The behavior of $x_s(\tau)$ and $\epsilon_s(\tau)$ for τ close to τ_c is also remarkable. The curves of these quantities, as shown in Fig. 8, are peculiar to second-order phase transitions. The dependence of $x_s(\tau)$ and $\epsilon_s(\tau)$ in the neighborhood of τ_c is governed by familiar laws of the type

$$x_s\propto\left[1-\frac{\tau_c}{\tau}\right]^n x,\quad \epsilon_s\propto\left[1-\frac{\tau_c}{\tau}\right]^\nu\epsilon\ , \tag{3.5}$$

respectively, where ν_x and ν_ϵ are critical exponents. This property is evident in the log-log plots of Fig. 8. Within the accuracy of our numerical analysis ν_x and ν_ϵ are equal. Most notably, for finite D they are always smaller than, but close to $\frac{1}{2}$. Note that $\frac{1}{2}$ is, in fact, the critical exponent of $x(\tau)$ given by Eq. (3.4). The investigations using both methods become difficult for small D so that

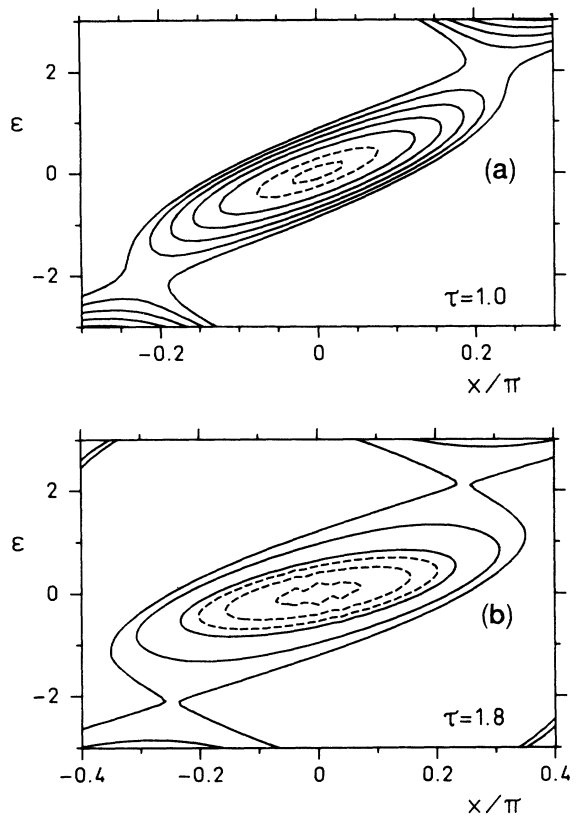

FIG. 9. Magnification of the holes of $P_0(x,\epsilon)$ taken from Fig. 2 for (a) $\tau=1.0$ and (b) $\tau=1.8$. The probability densities on the contours are as follows. Dashed: 1.95 and 2×10^{-3}, and solid: 2.1, 2.2, and 2.5×10^{-3}.

results for the critical exponents are not reliable.

The asymptotic behavior of $\epsilon_s(\tau)$ is largely an open problem. All of the data collected support our guess that $\epsilon_s(\tau)$ attains a finite value $\epsilon_s(\infty)$ for asymptotically large values of τ. Unfortunately, we did not achieve high enough accuracy to answer at least the question as to whether (and how) $\epsilon_s(\infty)$ depends on the noise intensity. We shall further touch this point in Sec. IV.

Finally, in Fig. 9, we take a closer look at the contour lines inside the hole. Such curves resemble a family of nested ellipses, the major axes of which rotate clockwise with the contour shrinking more closely around the origin. In the neighborhood of the origin (0,0), these ellipses all line up on the same direction, which, for increasingly large τ values and with D fixed, turns closer toward the x axis.

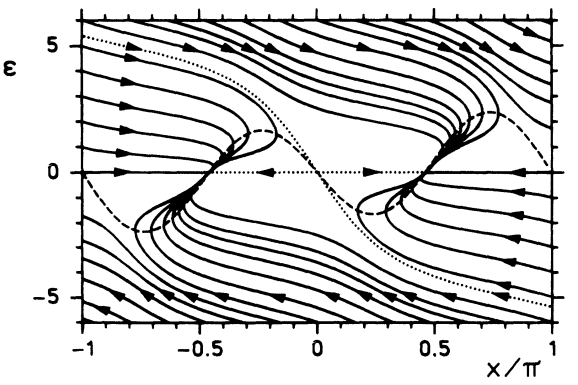

FIG. 10. Deterministic flow given by Eqs. (1.1) and (1.3) at $\tau=1$ for the potential shown in Fig. 1. The separatrix $\epsilon_x(x)$ (dotted) and the nodal curve $\epsilon_T(x)$ (dashed) are also plotted.

IV. CONCLUDING REMARKS

We hope that our study of the two-dimensional process described by Eqs. (1.1) and (1.3) may help to shed light on the debated problem of the escape dynamics in bistable potentials driven by colored noise.[5–15] In fact, the appearance of a hole in the stationary distribution implies that the most probable escape trajectory from one well into the other no longer runs through the origin, but instead crosses the border line between the two basins of attraction centered on $(x_0,0)$ along an off-axis path.

To clarify this property of the escape process, we follow the approach outlined in Ref. 15. In Fig. 10, we depict an example of deterministic flow in the periodic bistable potential, obtained by solving numerically Eqs. (1.1) and (1.3) after setting $\Gamma(t)\equiv0$. The separatrix curve $\epsilon_x(x)$, dividing the two basins of attraction, is represented by a dotted line. The turning points of the flow lines are determined by the equation $dx/d\epsilon=0$, and from the nodal curve

$$\epsilon_T(x)=f'(x)\ . \tag{4.1}$$

For large values of τ, $\epsilon_T(x)$ and $\epsilon_x(x)$ come very close to one another, in the domain $|x|<\tilde{x}_\infty$, rendering it unlikely for the flow lines to approach the origin. On the other hand, deterministic flow lines run almost parallel to the separatrix for a long distance, so that even a small exter-

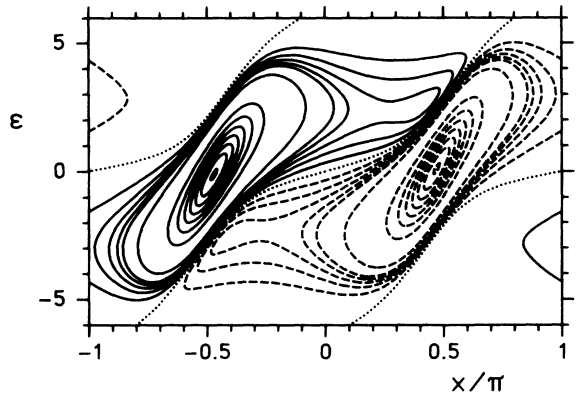

FIG. 11. $P_1(x,\epsilon)$ contour lines for the same conditions of Fig. 10 in the presence of noise $\Gamma(t)$ with $D=3$. The probability densities on the contour lines are as follows. Solid: $1\times10^3, 2\times10^3, \ldots, 5\times10^3, 1\times10^4, 6\times10^4, \ldots, 3.6\times10^5$; dashed: negative but with the same absolute values as the positives. All probability densities are normalized with respect to the separatrix, shown dotted, which has been assigned the value zero.

nal noise might happen to kick a flow line over the separatrix into the adjacent basin before it reaches the top of the potential barrier at $x_u=0$. The region where such a mechanism is more likely to take place is the domain in the phase space (x,ϵ) encompassed by the separatrix and the extremal points $\pm\bar{x}_\infty$ of the nodal curve[15] [see Eq. (3.4)].

We verified this picture of the escape processes driven by strongly colored noise by monitoring the eigenfunction of the spectral equation (2.5) corresponding to the smallest nonzero eigenvalue, $P_1(x,\epsilon)$. An example is shown in Fig. 11. Under the action of the additive noise $\Gamma(t)$, the trajectories of the two-dimensional process leak out of one basin of attraction into the other. The escape path runs from $(-|x_0|,0)$ to $(|x_0|,0)$ through s_+ and back from $(|x_0|,0)$ to $(-|x_0|,0)$ through s_-. In this respect, the saddle points $s_\pm$ are nonsymmetric. The relevant stochastic escape trajectories in the phase space (x,ϵ) have also been obtained recently by Lindenberg and co-workers[22] by means of a digital simulation, thus leading to the same phenomenological description of the escape mechanism.

It is clear now why we have attached so much importance to the question of locating $s_\pm$ with varying τ. The analytical determination of the curve $x_s(\tau)$ and $\epsilon_s(\tau)$ would amount to solving the problem of the τ dependence of the relevant escape times.[10–15] Conversely, following the line of reasoning expounded in Ref. 15, we can get a clue to the existence of the asymptotic limit $\epsilon_s(\infty)$. Having already noticed that the most probable escape trajectory must run through an off-axis saddle point, we can make use of the fact that for $\tau\to\infty$ the separatrix approximates the line

$$\lim_{\tau\to\infty}\epsilon_x(x)=\begin{cases}\epsilon_T(x), & |x|\le\bar{x}_\infty\\ \pm\epsilon_T(\bar{x}_\infty), & \pm x>\bar{x}_\infty\end{cases} \tag{4.2}$$

to suggest that $\epsilon_s(\infty)$ is likely to coincide with $\epsilon_T(\bar{x}_\infty)=f''(\bar{x}_\infty)$, at least for vanishingly small D and asymptotically large τ. For the sake of comparison with the results displayed in Fig. 8, we report the predicted values of $x_s(\infty)$ and $\epsilon_s(\infty)$ for the potential of Fig. 1, namely $x_s(\infty)=0.739$ and $\epsilon_s(\infty)=1.655$. The convergence of $\epsilon_s(\tau)$ to its expected asymptotic value, if confirmed, would turn out to be very slow (see Fig. 8). However, such a behavior would be consistent with the slow convergence of the relevant escape rate toward its estimated asymptotic value.[14,15]

ACKNOWLEDGMENTS

We wish to thank P. Hänggi, P. Jung, and L. Schimansky-Geier for valuable discussions. This work was supported in part by the Consiglio Nazionale delle Ricerche (CNR-CISM), the Deutsche Forschungsgemeinschaft (DFG), NATO Grant No. 0770/85, and by the Office of Naval Research, Grant No. N00014-88-K-0084.

*Present address: Department of Electrical Engineering, Michigan State University, East Lansing, MI.

†Present address: Analytische Philosophie/Wissenshaftstheorie, Universität Augsburg, D-8900 Augsburg, Federal Republic of Germany.

[1]R. L. Stratonovich, *Topics in the Theory of Random Noise* (Gordon and Breach, New York, 1967), Vol. I.

[2]H. Haken, *Synergetics* (Springer, Berlin, 1983).

[3]H. Risken, *The Fokker-Planck Equation,* 2nd ed. (Springer, Berlin, 1989).

[4]*Noise in Nonlinear Dynamical Systems,* edited by F. Moss and P. V. E. McClintock (Cambridge University Press, Cambridge, England, 1989).

[5]H. A. Kramers, Physica **7**, 284 (1940).

[6]See the review articles in Vol. 1 of Ref. 4.

[7]Th. Leiber and H. Risken, Phys. Rev. A **38**, 3789 (1988).

[8]P. Hänggi, F. Marchesoni, and P. Grigolini, Z. Phys. B **56**, 333 (1984).

[9]M. M. Blosek-Dygas, B. J. Matkowsky, and Z. Schuss, Phys. Rev. A **38**, 2605 (1988).

[10]Th. Leiber, F. Marchesoni, and H. Risken, Phys. Rev. Lett. **59**, 1381 (1987), **60**, 59(E) (1988); Phys. Rev. A **38**, 982 (1988).

[11]G. P. Tsironis and P. Grigolini, Phys. Rev. Lett. **61**, 7 (1988).

[12]P. Jung and P. Hänggi, Phys. Rev. Lett. **61**, 11 (1988).

[13]J. F. Luciani and A. D. Verga, Europhys. Lett. **4**, 255 (1987).

[14]A. J. Bray and A. J. McKane, Phys. Rev. Lett. **62**, 493 (1989); A. J. McKane, H. C. Luckock, and H. J. Bray, Rev. A **41**, 664 (1990); A. J. Bray, A. J. McKane, and T. J. Newman, *ibid.* **41**, 657 (1990).

[15]P. Hänggi, P. Jung, and F. Marchesoni, J. Stat. Phys. **54**, 1367 (1989).

[16]P. Jung and H. Risken, Z. Phys. B **61**, 367 (1985).

[17]F. Moss and P. V. E. McClintock, Z. Phys. B **61**, 381 (1985).

[18]F. Marchesoni and F. Moss, Phys. Lett. A **131**, 322 (1988).

[19]G. Debnath, F. Moss, F. Marchesoni, Th. Leiber, and H. Risken, J. Stat. Phys. **54**, 1381 (1989).

[20]See Ref. 4, Vol. 3, Chap. 9.

[21]W. Horsthemke and R. Lefever, *Noise Induced Transitions* (Springer-Verlag, Berlin, 1984).

[22]L. Ramirez-Piscina, J. M. Sancho, F. J. de la Rubia, K. Lindenberg, and G. P. Tsironis, Phys. Rev. A **40**, 2120 (1989); K. Lindenberg, L. Ramirez-Piscina, J. M. Sancho, and F. J. de la Rubia, *ibid.* **40**, 4157 (1989).

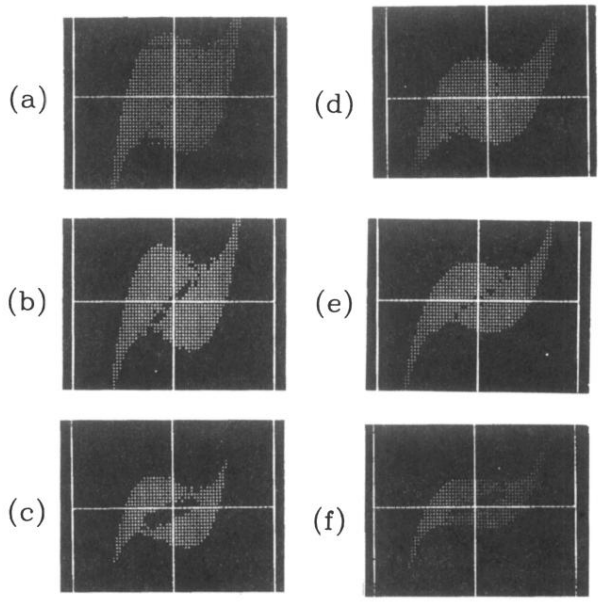

FIG. 5. $P_0(x,\epsilon)$ cross section through the saddle point for the potential shown in Fig. 4 measured on the analog simulator for $\tau=5$: (a) $D=2.2>D_c$, (b) $D=2.1\cong D_c$, and (c) $D=0.45<D_c$; and for $\tau=10$: (d) $D=48.4>D_c$, (e) $D=22.5\simeq D_c$ and (f) $D=6.4<D_c$.